Available online at www.sciencedirect.com
ScienceDirect
Trans. Nonferrous Met. Soc. China 33(2023) 3266−3281
Transactions of Nonferrous Metals Society of China
www.tnmsc.cn

Effect of single roll drive rolling on microstructure, texture, and mechanical property anisotropy of Al−5.6Zn−2.5Mg−1.4Cu aluminum alloy

Amir KAZEMI-NAVAEE, Roohollah JAMAATI, Hamed JAMSHIDI AVAL

Department of Materials Engineering, Babol Noshirvani University of Technology, Shariati Ave., Babol 47148–71167, Iran

Received 19 April 2022; accepted 16 August 2022

Abstract: The current research aimed to study the microstructure and texture development of the Al−5.6Zn−2.5Mg−1.4Cu alloy during single roll drive rolling process (SRDR). The relationship between mechanical property anisotropy and microstructure and texture was investigated in detail. The SRDR process was immediately performed on the solution-treated sample with four different thickness reductions of 10%, 20%, 40%, and 60%, respectively. Microstructural examination by optical and scanning electron microscopes, texture evaluation by X-ray diffraction, and mechanical properties evaluation by tensile tests were conducted. The results showed that the value of in-plane anisotropy was significantly reduced from 11.6% in solution-treated alloy to 2.4% and 3.1% in 40% and 60% reduction rolled samples, respectively. This was due to the formation of the Rotated Cube component, decreasing the overall texture intensity, and the formation of new grains through dynamic recrystallization. The yield strength in the rolling direction (RD) was higher than that in the transverse direction (TD), which was due to grain morphology and texture in these samples. The severity of Portevin−Le Chatelier (PLC) along the RD (0°) was much lower than that along the HD (45°) and TD (90°) owing to the presence of several strong orientations along the RD. By increasing the thickness reduction, the difference between strain hardening rates of RD, HD, and TD decreased due to the decrement of texture intensity. There was no difference between the fracture surfaces of 60% samples in the RD, HD, and TD, revealing nearly isotropic fracture behavior.

Key words: AA7075 aluminum alloy; single roll drive rolling; texture; mechanical properties; anisotropy

1 Introduction

Aluminum and its alloys are widely used in the aerospace, marine, automotive, packaging, and construction industries. The 7xxx series aluminum alloys are precipitation-hardened alloys and their strength mainly depends on $MgZn_2$ precipitates. These alloys, owing to their high specific strength and good corrosion resistance, are used in the automotive and aerospace industries. As a result, controlling their properties is very important [1−4].

In the plastic deformation of materials, the orientation of grains often changes. The preferred orientation of grains (texture) requires to be controlled because it has a remarkable impact on anisotropy (i.e. variations in properties with direction) [5]. The in-plane anisotropy (IPA) in percentage has been used in the literature to quantify anisotropy based on yield stress in engineering stress−strain curves in three different directions viz 0°, 45°, and 90° to the rolling direction [6,7]. Anisotropy in yield stress by a novel thermo-mechanical treatment on AA7075 alloy, investigated by HUO et al [8], has been greatly decreased and the difference between yield stress in the RD and TD was only 2 MPa.

Another process that led to decreasing the anisotropy was the hot cross-rolling process

Corresponding author: Roohollah JAMAATI, E-mail: jamaati@nit.ac.ir
DOI: 10.1016/S1003-6326(23)66332-0
1003-6326/© 2023 The Nonferrous Metals Society of China. Published by Elsevier Ltd & Science Press

performed by MONDAL et al [7] on AA7010 alloy. The results showed the degree of IPA in peak-aged cross rolled alloy, in spite of having strong rotated brass, was the lowest, equal to 2.28%. It has been proved that IPA of the present alloy was affected directly by the texture. Cold rolling followed by annealing on AA7075 alloy was investigated by TAJALLY and EMADODDIN [9]. Their results showed that the sample which was cold rolled to 71% thickness reduction followed by annealing at 350 °C for 5 min had good ductility and low anisotropy. The effect of cross rolling and post-deformation heat treatment on AA7075 alloy was investigated by LI et al [10]. It was found that the mentioned process reduced the intensity of the important texture components including Copper, S, and Brass. Moreover, this process significantly decreased the anisotropy value of tensile properties. The effect of the cross-rolling process and T6 temper on the anisotropy of Al−Cu−Li aluminum alloy was investigated by NAYAN et al [6]. The as-rolled sample exhibited a high Brass texture component with high IPA whereas the as-tempered sample showed very low maximum texture intensity with very low IPA. In fact, by decreasing the maximum texture intensity, the degree of anisotropy has decreased.

In general, anisotropy is caused by texture and morphological features including grain and particle shape. However, the texture has higher importance in controlling the anisotropy of aluminum alloys [7]. It was reported that asymmetric rolling by the single roll drive rolling (SRDR) method produced a non-conventional deformation texture in metals and alloys [11−21]. However, the experimental studies conducted on SRDR of aluminum alloys are limited in literature, and no investigations were carried out on the effect of SRDR on the mechanical properties anisotropy of materials. Therefore, the SRDR technique on the AA7075 alloy was performed in the present work. The current research aimed to study the microstructure and texture development during SRDR of the AA7075 alloy. The relationship between anisotropy with microstructure and texture was investigated in detail.

2 Experimental

A plate with dimensions of 100 mm × 50 mm × 10 mm of commercial AA7075-T651 alloy was used. The chemical composition of AA7075 alloy is listed in Table 1. The plate was then exposed to a solution treatment (480 °C, 6 h) using an induction furnace under an air atmosphere followed by quenching in water. This sample was selected as the 0% sample. The asymmetric cold rolling process was immediately performed on the solution-treated sample with four different thickness reductions of 10%, 20%, 40%, and 60% using the SRDR technique. The schematic of the SRDR is presented in Fig. 1. The width and diameter of the rolls were 200 and 150 mm, respectively.

Table 1 Chemical composition of alloy (wt.%)

Zn	Mg	Cu	Fe	Cr	Al
5.63	2.50	1.44	0.22	0.21	Bal.

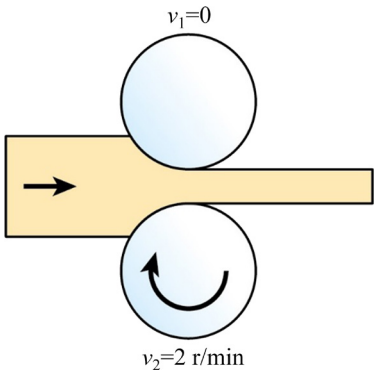

Fig. 1 Schematic illustration of SRDR

The preparation of samples for metallographic examinations was conducted by conventional polishing on a series of sandpapers followed by disc polishing using dilute alumina suspension. The samples for optical microscopy (OM) observations were cut from all three planes, i.e. RD−TD, TD−ND, and RD−ND planes. Microstructural images on RD−TD, RD−ND, and TD−ND planes were studied by optical microscopy using Keller's etchant (distilled water + HNO_3 + HCl + HF). The bulk texture analysis of the samples in half-thickness on the RD−TD plane was performed using an Xpert Pro (PANalytical) device with Cr K_α radiation. Inverse pole figures (IPFs) and orientation distribution functions (ODFs) were calculated by TexTools software.

The tensile properties of the solution-treated and rolled samples were evaluated using the 18 mm gauge length flat tensile sample in longitudinal (RD), transverse (TD), and 45° to rolling direction

(HD). The schematic illustration of the tensile test in three different directions is depicted in Fig. 2. For repeatability, the tensile test was conducted twice in each direction. The tests were conducted according to the ASTM E8 standard at room temperature using the Santam machine with a 1 mm/min crosshead speed. Scanning electron microscopy (SEM) observation was performed to investigate the fracture surface of the samples.

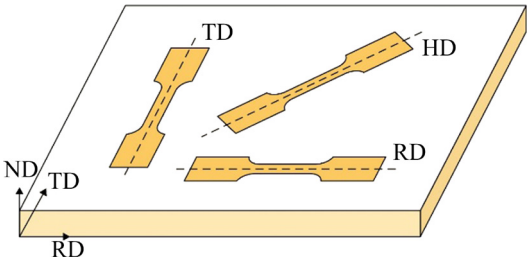

Fig. 2 Schematic illustration of tensile samples in three different directions

3 Results and discussion

3.1 Microstructure and texture

The optical microstructures and IPFs of the solution-treated and deformed AA7075 alloys, i.e. 0%, 10%, 20%, 40%, and 60% samples, are presented in Figs. 3–7, respectively. As can be seen in Fig. 3, the grains are coarse and the shape of the grains is elongated, which is due to the retention of the previous structure by rolling. As can be seen in Figs. 3(b), (d), and (f), the 0% sample exhibited [112]//ND, [001]//ND, [110]//TD, [110]//RD, [001]//RD, [103]//RD, and [102]//RD orientations with the maximum texture intensity of 2.0, 1.4, 1.8, 1.2, 1.1, 1.2, and 1.2 (multiple of random distribution), respectively. By 10% and 20% rolling, the grains become more elongated along RD (Figs. 4 and 5) and the grain size is reduced. In the 10% rolled sample, [111]//ND is formed, [112]//ND is strengthened, and other orientations are weakened. The 10% rolled sample has [112]//ND, [111]//ND, [110]//TD, and [110]//RD orientations with the maximum intensity of 2.1, 1.6, 1.3, and 1.2, respectively. The 20% rolled sample exhibits [112]//ND, [001]//ND, [111]//ND, [110]//TD, [215]//RD, and [103]//RD orientations with the maximum texture intensity of 1.6, 1.1, 1.2, 1.5, 1.2, and 1.2, respectively. After 40% thickness reduction,

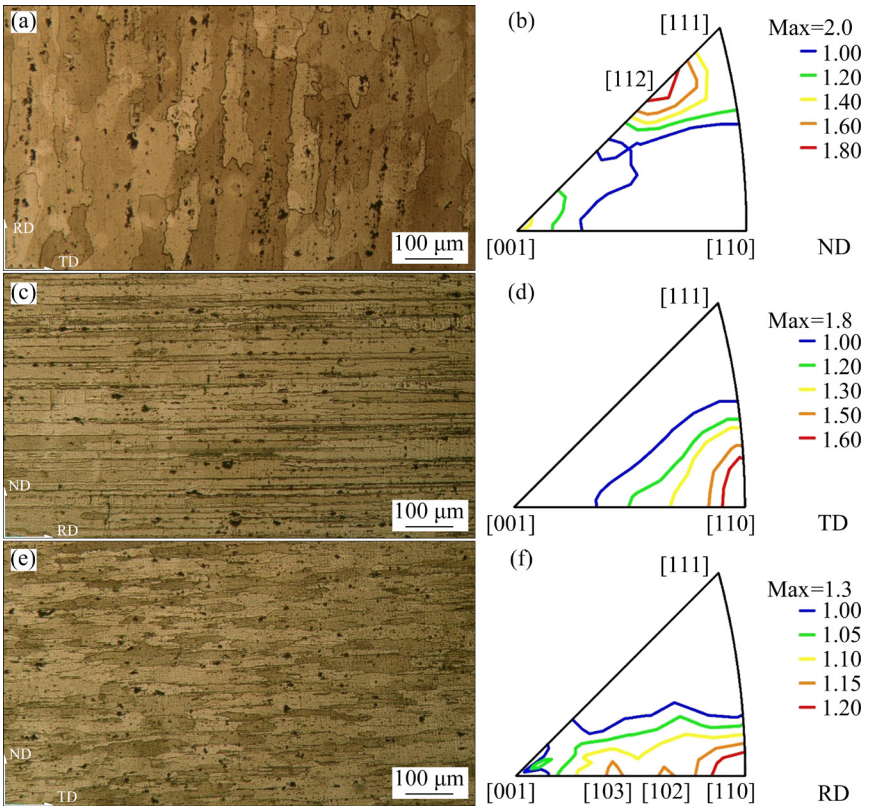

Fig. 3 OM images (a, c, e) and IPFs (b, d, f) of solution-treated alloy (0% sample) in RD−TD (a, b), RD−ND (c, d), and TD−ND (e, f) planes

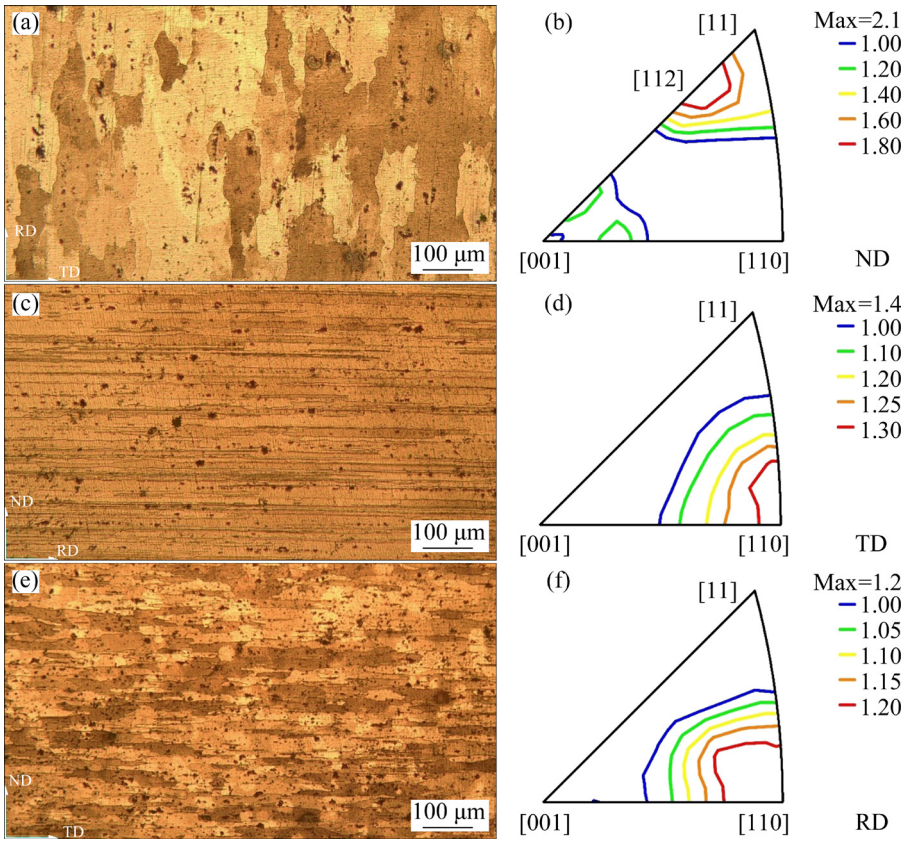

Fig. 4 OM images (a, c, e) and IPFs (b, d, f) of 10% rolled alloy in RD−TD (a, b), RD−ND (c, d), and TD−ND (e, f) planes

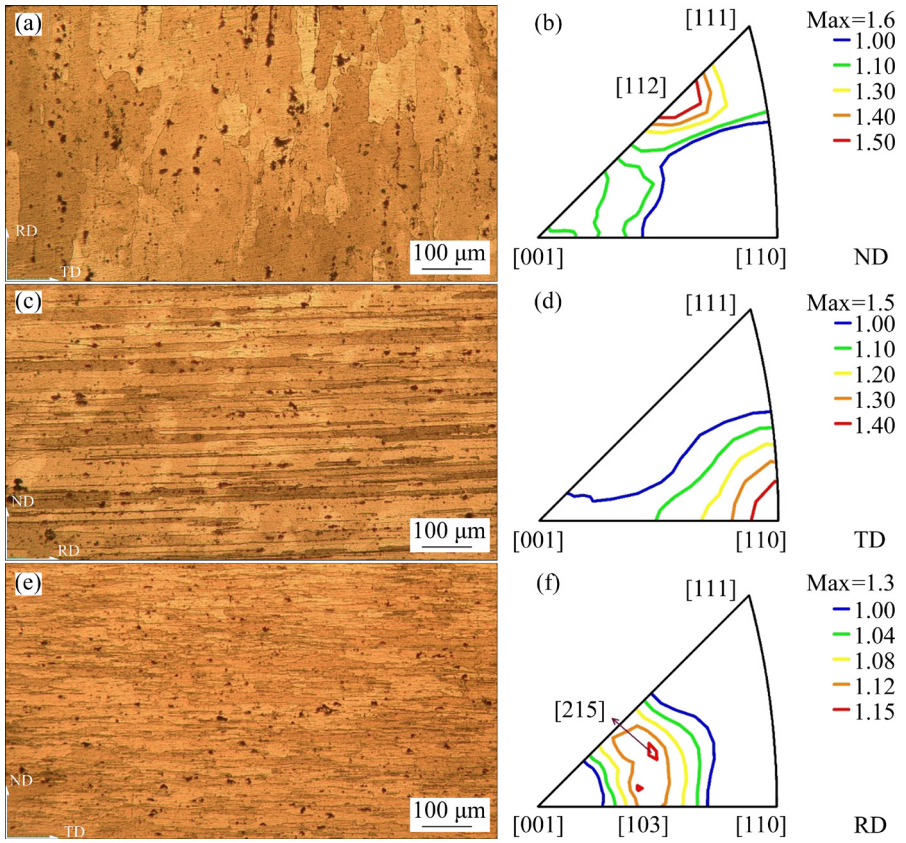

Fig. 5 OM images (a, c, e) and IPFs (b, d, f) of 20% rolled alloy in RD−TD (a, b), RD−ND (c, d), and TD−ND (e, f) planes

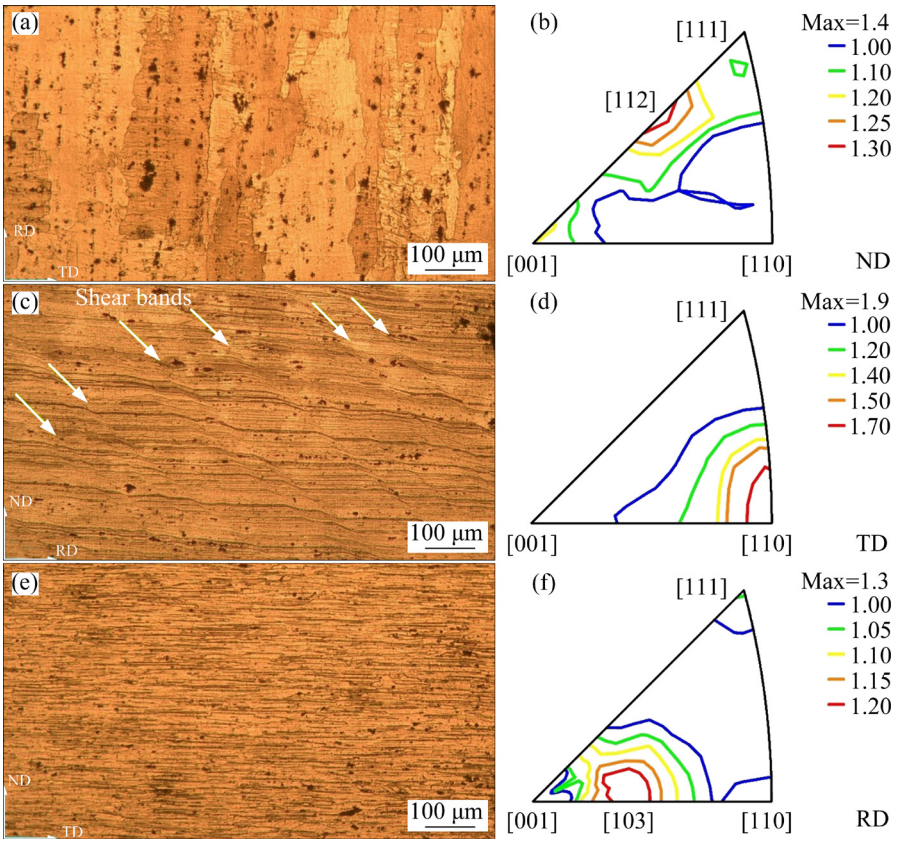

Fig. 6 OM images (a, c, e) and IPFs (b, d, f) of 40% rolled alloy in RD−TD (a, b), RD−ND (c, d), and TD−ND (e, f) planes

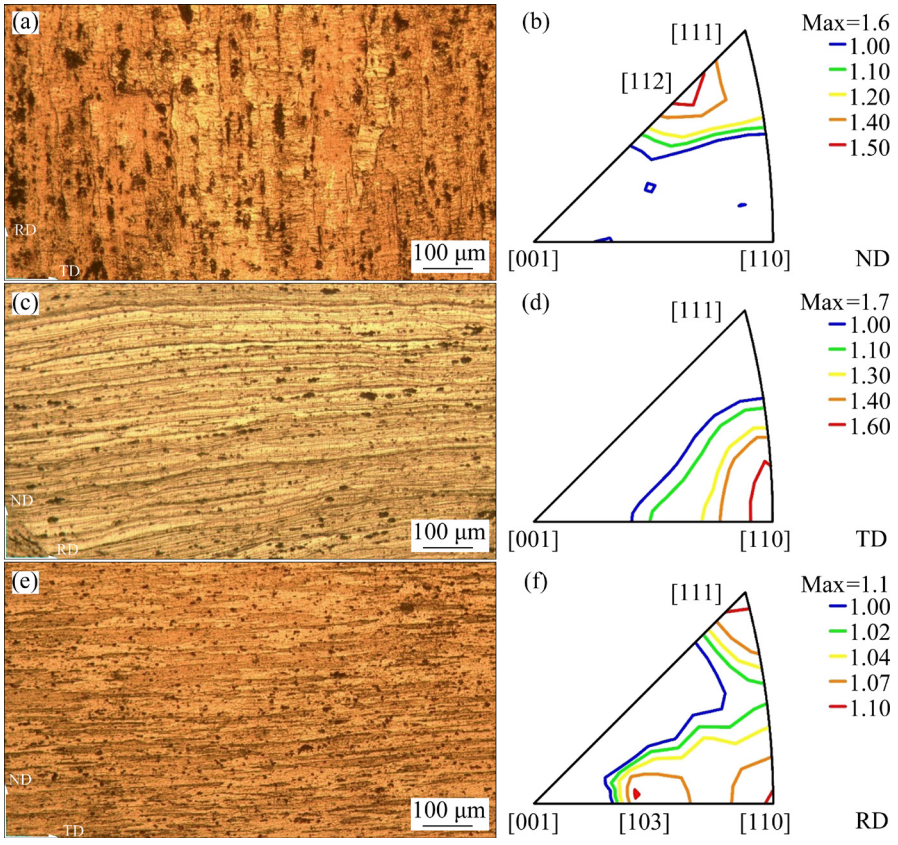

Fig. 7 OM images (a, c, e) and IPFs (b, d, f) of 60% rolled alloy in RD−TD (a, b), RD−ND (c, d), and TD−ND (e, f) planes

the grain width is decreased and shear bands are formed which are easily visible in the RD−ND plane (as indicated by green arrows in Fig. 6(c)). [112]//ND, [111]//ND, [001]//ND, [110]//TD, and [103]//RD, with maximum texture intensities of 1.4, 1.2, 1.2, 1.9, and 1.3 are the texture components of 40% rolled sample, respectively. Finally, by rolling up to the highest possible amount, i. e. 60% thickness reduction, the grain widths are significantly decreased. As seen in Fig. 7, shear bands are formed in this sample, too. [112]//ND, [111]//ND, [110]//TD, [103]//RD, [110]//RD, and [111]//RD with the maximum intensities of 1.6, 1.4, 1.7, 1.1, 1.1, and 1.1 are the texture components of 60% rolled sample, respectively.

One of the most important effects of the rolling process on the microstructure of AA7075 alloy is the fragmentation of intermetallic particles. Figure 8 shows the fracture of intermetallic particles after the 20% and 40% SRDR process. The brittle intermetallic particles are weak in shear stress. Consequently, during SRDR process, these particles are fractured and fragmented. It should be noted that the distribution of fragmented particles is not uniform at the low level of deformation. However, with increasing the thickness reduction to 60%, the distance between the fragmented particles increases, and a better distribution of particles in the aluminum matrix can be observed in both different planes, as shown in Fig. 9.

The ODFs of solution-treated and rolled samples are presented in Fig. 10. In the solution-

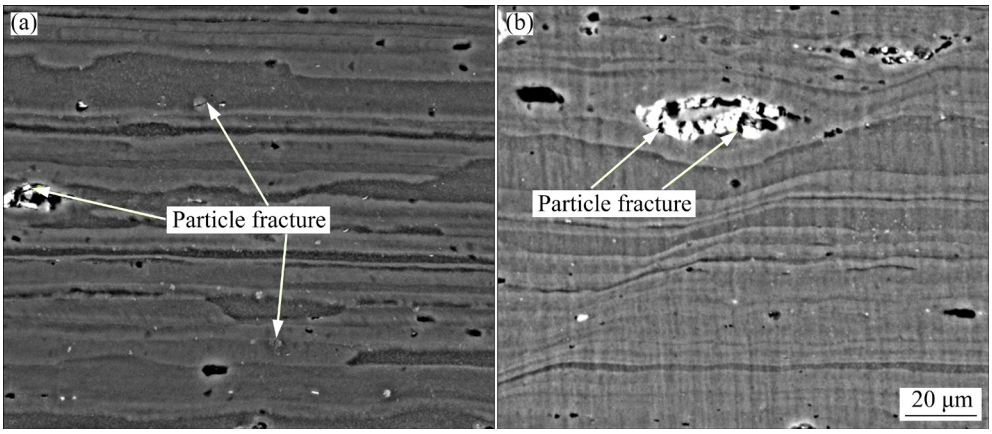

Fig. 8 SEM images of 20% (a) and 40% (b) rolled samples in RD−ND plane

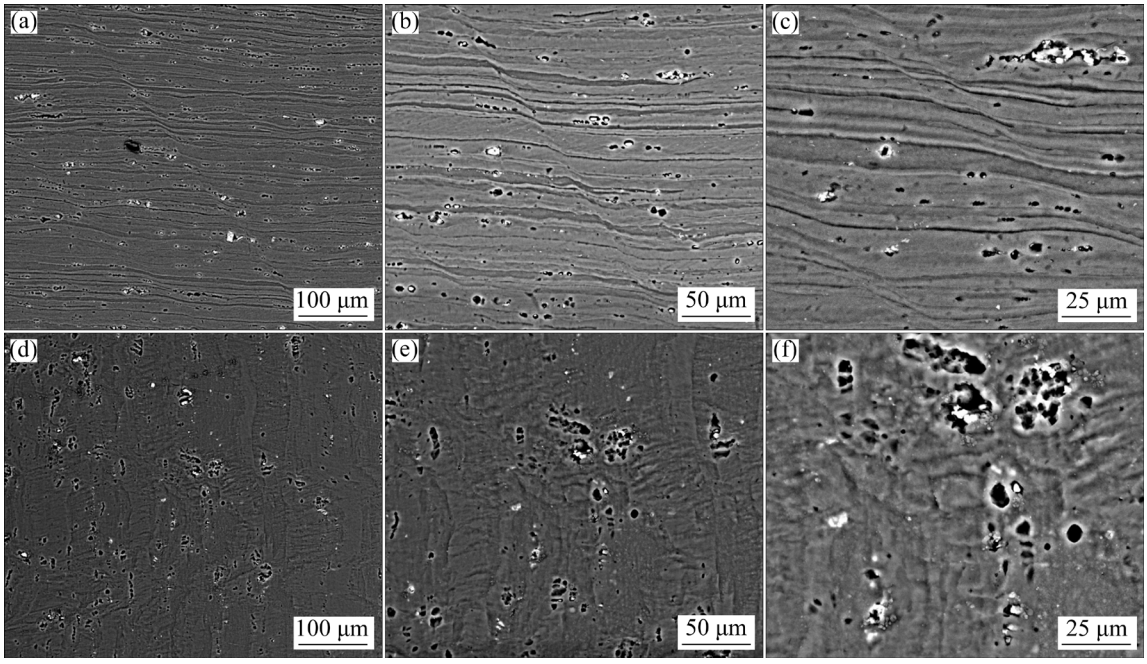

Fig. 9 SEM images of 60% rolled sample in RD−ND (a, b, c) and RD−TD (d, e, f) planes

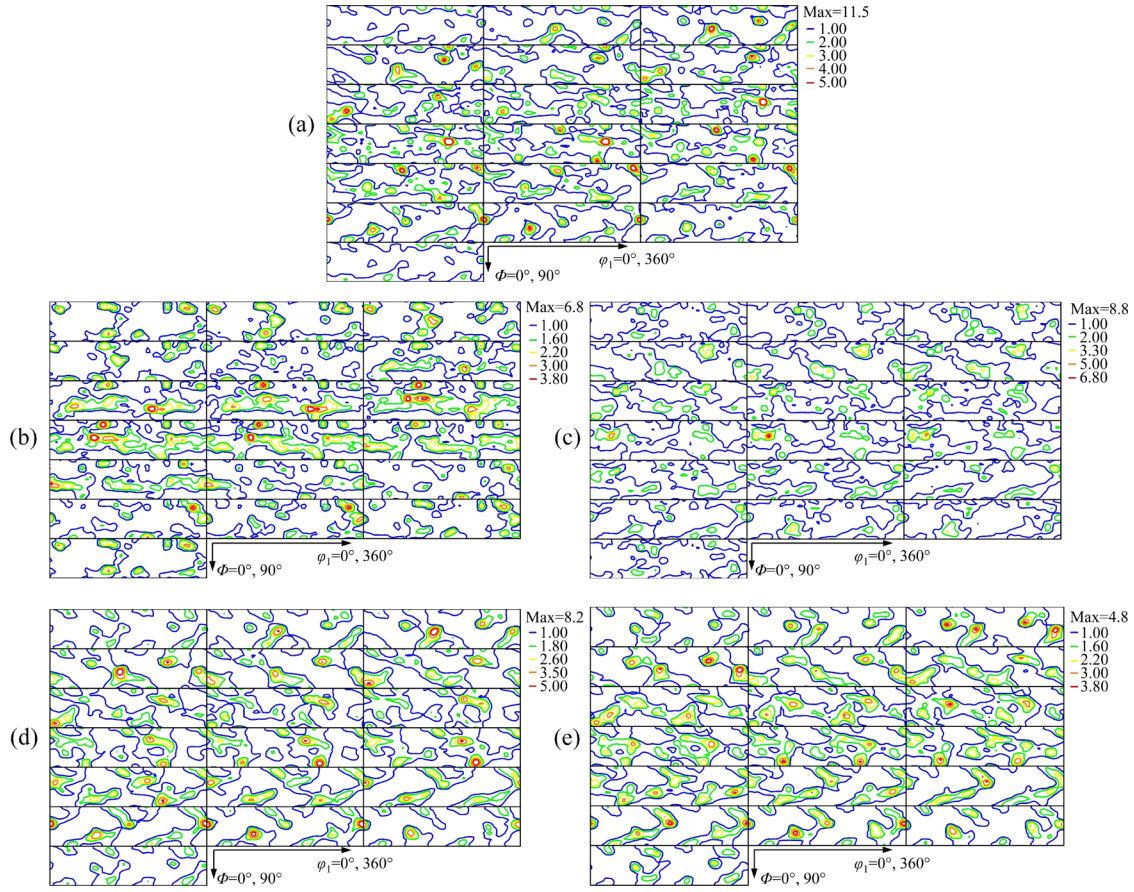

Fig. 10 ODFs of 0% (solution-treated) (a), 10% (b), 20% (c), 40% (d), and 60% (e) rolled samples

treated sample (Fig. 10(a)), the maximum texture intensity is the highest compared to other samples, equal to 11.5. The intensest components in this sample are Rotated Copper and Goss with a maximum intensity of 3.2 and 2.7, respectively. The maximum texture intensity in 10% and 20% rolled samples is reduced to 6.8 and 8.8 as compared to the solution-treated sample. The intensest texture components are Rotated Copper and S, with the maximum intensity of 2.0 and 2.6, for the 10% and 20% rolled samples, respectively. In the 40% rolled sample, the maximum texture intensity is 8.2. Three texture components, i.e. Rotated Cube, Goss, and Brass with the maximum intensity of 3.0, 2.9, and 1.8, respectively, have the highest intensity in the 40% rolled sample compared to other samples. The maximum texture intensity is significantly decreased to 4.8 in the 60% rolled sample. The intensest texture component in this sample is the Copper with an intensity of 2.7.

It is interesting to note that the intensity of Goss, as a recrystallization texture component, remarkably increases in the 40% and 60% samples, indicating the occurrence of dynamic recrystallization. To confirm this, the SEM image of the 60% rolled sample at high magnification is depicted in Fig. 11. Several new grains can be observed within the original grains. The recrystallization texture of most aluminum alloys is characterized by the Cube orientation with some scatter about the rolling direction (RD) towards the

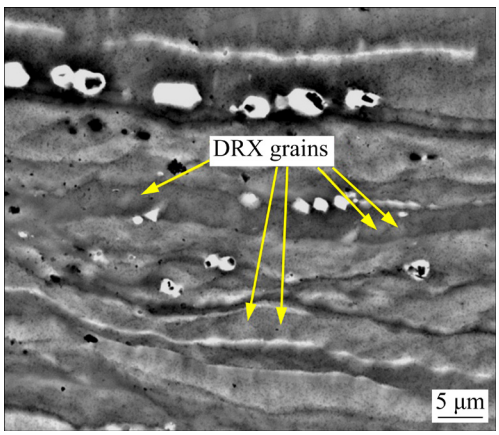

Fig. 11 SEM image of AA7075 alloy after 60% asymmetric cold rolling

Goss orientation [22−24]. Therefore, the new grains can be responsible for strengthening the Goss components after the 40% and 60% asymmetric cold rolling. It was reported that at the beginning of recrystallization, Goss-oriented grains nucleate preferentially at the shear bands [25,26]. The formation of these grains is effective on the tensile behavior and anisotropy in the AA7075 alloy which will be discussed later.

Based on the microstructure and texture results, it can be concluded that with increasing the rolling reduction, the width of grains decreases, and the number of shear bands increases. Also, the overall intensity of texture decreases due to performing the asymmetric rolling.

3.2 Anisotropy in mechanical properties

The tensile properties of materials depend directly on Young's modulus in the given direction. The Einstein summation is widely used to describe the elastic behavior of anisotropic materials [27]. The shorthand form of this notation is $\varepsilon_i=S_{ij}\sigma_j$, where ε_i is the strain, S_{ij} is the compliance constant, σ_j is the stress, and a 6 × 6 S_{ij} matrix substitutes for the matrix of elastic constants. In Einstein's notation, it is understood that summation over all j=1−6 is implied for each i value [27]. Cubic materials have three axes separated by $\alpha=\beta=\gamma=90°$, but the three axes are elastically equivalent. This means that $S_{11}=S_{22}=S_{33}$, $S_{44}=S_{55}=S_{66}$, and $S_{12}=S_{13}=S_{23}$, so a table describing cubic materials needs only to report the three independent S_{11}, S_{12}, and S_{44} values [27]. To calculate Young's modulus of any alloy in any direction, the following formula is used [27]:

$$\frac{1}{E_{hkl}}=S_{11}-2\left[S_{11}-S_{12}-\frac{S_{44}}{2}\right]\left(l_1^2l_2^2+l_2^2l_3^2+l_1^2l_3^2\right) \quad (1)$$

where E_{hkl}, S, and l are Young's modulus in [hkl] direction, compliance constant, and direction cosine, respectively. Direction cosine values for the principal crystallographic directions in the cubic lattice are given in Table 2. According to Eq. (1), the elastic modulus of alloys is dependent on the three independent elastic constants (S_{11}, S_{12}, and S_{44}) and the direction cosine values (l_1, l_2, and l_3) of the crystallographic direction under study. The magnitudes of elastic constants, i.e. S_{11}, S_{12} and S_{44}, for aluminum are 1.57×10^{-11}, -0.57×10^{-11}, and 3.51×10^{-11} Pa^{-1}, respectively [27]. The values of $l_1^2l_2^2+l_2^2l_3^2+l_1^2l_3^2$ along with elastic modulus of aluminum in the strong important directions which are evident in the IPFs of the AA7075 alloy (Figs. 3−7) are listed in Table 3 (Eq. (1) is used for calculations). As a result, by strengthening the directions in which the elastic modulus is high such as [111], the tensile properties in that direction will be increased. On the other hand, by increasing the intensity of the weaker orientation such as [100], the tensile properties will be decreased.

Table 2 Direction cosines for main directions in cubic crystal system [27]

Direction	l_1	l_2	l_3
⟨100⟩	1	0	0
⟨110⟩	$2^{-0.5}$	$2^{-0.5}$	0
⟨111⟩	$3^{-0.5}$	$3^{-0.5}$	$3^{-0.5}$

Table 3 Values of $l_1^2l_2^2+l_2^2l_3^2+l_1^2l_3^2$ along with elastic modulus for aluminum for some important orientations in present work

Direction	$l_1^2l_2^2+l_2^2l_3^2+l_1^2l_3^2$	E/GPa
[100]	0	63.7
[103]	9/100	66.6
[215]	43/300	68.5
[102]	4/25	69.1
[112]	1/4	72.6
[110]	1/4	72.6
[111]	1/3	76.1

Cube, Goss, Brass, Copper, S, Rotated Cube, and Rotated Copper are the important texture components in the present work. The strengthening or weakening of these texture components is very important in the amount of anisotropy. The intensity of these components is listed in Table 4. The rolling texture is shown as {hkl}⟨uvw⟩. This means the [hkl] of many grains is parallel to ND and [uvw] of many grains is parallel to RD. To calculate the third orientation, i.e. the orientation parallel to TD, it is just needed to calculate the exterior product of [hkl] and [uvw]. These calculations are performed for the important components and the results are listed in Table 5. For example, if Goss orientation is increased in a sample, it means that [110] of many grains is parallel to ND, [001] to RD, and [110] to TD. When it comes to tensile properties (comparing

Table 4 Intensity of main components

Thickness reduction/%	Copper	S	Brass	Cube	Rotated Cube	Goss	Rotated Copper
0	1.6673	1.4806	0.8130	1.4523	2.3690	2.6797	3.2201
10	1.9585	0.8966	1.3730	1.3609	1.6217	1.4980	1.9714
20	2.4879	2.5961	1.0805	1.8085	1.8897	1.7885	2.4616
40	2.3637	1.6992	1.7576	1.2207	2.9687	2.8884	1.7954
60	2.6952	1.2807	1.6260	1.1362	2.1883	1.9397	1.3900

Table 5 Important texture components with their orientation towards ND, RD, and TD

Component	ND	RD	TD
Cube	⟨001⟩	⟨100⟩	⟨010⟩
Goss	⟨110⟩	⟨001⟩	⟨110⟩
Brass	⟨110⟩	⟨112⟩	⟨111⟩
Copper	⟨112⟩	⟨111⟩	⟨110⟩
S	⟨123⟩	⟨634⟩	⟨17 22 8⟩
Rotated Cube	⟨001⟩	⟨110⟩	⟨110⟩
Rotated Copper	⟨112⟩	⟨110⟩	⟨111⟩

properties in RD and TD), intensifying Copper component and weakening Goss, Brass, and Rotated Copper components lead to strengthening tensile properties in the RD direction. On the other hand, intensifying Goss, Brass, and Rotated Copper components and weakening Copper component lead to strengthening tensile properties in TD. The important point is that increasing the intensity of Cube and Rotated Cube texture components leads to the equality of tensile properties in two directions of RD and TD. In fact, intensifying Cube and Rotated Cube texture components leads to a decrease in the anisotropy of mechanical properties.

The engineering stress−strain curves of solution-treated and rolled alloys in three different directions (RD, HD, and TD) are presented in Fig. 12. Also, the yield and ultimate tensile strengths (YS and UTS), and total elongation (TE) of all samples in three different directions are depicted in Fig. 13. The lowest values of YS (117.6 MPa) and UTS (348 MPa) and the highest value of TE (30.5%) belong to the 0% sample. This is due to the large grain size and lack of work hardening effect. Serrated SS curves of the 0% sample in three directions (Fig. 12(a)) are observed, which is due to the Portevin-Le Chatelier (PLC) effect. The occurrence of PLC can be ascribed to the presence of many solute atoms and low dislocation density in the solution-treated condition. In the solution-treated sample, the dislocations are more likely to be trapped by solute atoms. As a result, the probability of PLC increases.

As can be seen in Figs. 12 and 13, applying the SRDR process up to 60% thickness reduction leads to an increment of the YS and UTS and a decrement of the TE of the samples in all three directions. The highest values of YS and UTS were achieved in the 60% rolled sample, equal to 569 and 644 MPa, respectively. This can be attributed to the grain refinement and work hardening effect of the rolled samples. Besides, the fragmentation of intermetallic particles by rolling leads to increasing the strength of the alloy.

As seen in Fig. 13(a), in the solution-treated sample, the magnitude of yield stress in the RD is higher than that in the TD which could have two reasons. Firstly, this result is due to the presence of four orientations in the RD direction, i.e. [110], [102], [103], and [100] with the maximum intensity of 1.2, 1.2, 1.2, and 1.1 versus one orientation in TD, i.e. [110] with the maximum intensity of 1.8 (see Fig. 3). Secondly, the absence of the Brass component in this sample can be a reason for strong yield strength in the RD (see Fig. 10(a)). From Fig. 13(a), the amount of YS in the RD is higher than that in the TD, for 10% and 20% rolled samples, which is in good agreement with the previous research [28]. This may have a micro-structural reason. This can be attributed to the elongated grains in the RD owing to the rolling process (see Figs. 4 and 5). But this trend is completely reversed for the 40% rolled sample. It means the YS value in the TD is higher than that in the RD. This result can be ascribed to two main reasons. Firstly, the single orientation, i.e. [110], has an intensity of 1.9 in the TD; however, there is only an [103] orientation with an intensity of 1.3, which proves the dominance of the YS value in TD over RD (see Fig. 6 and Table 3). Secondly, TD

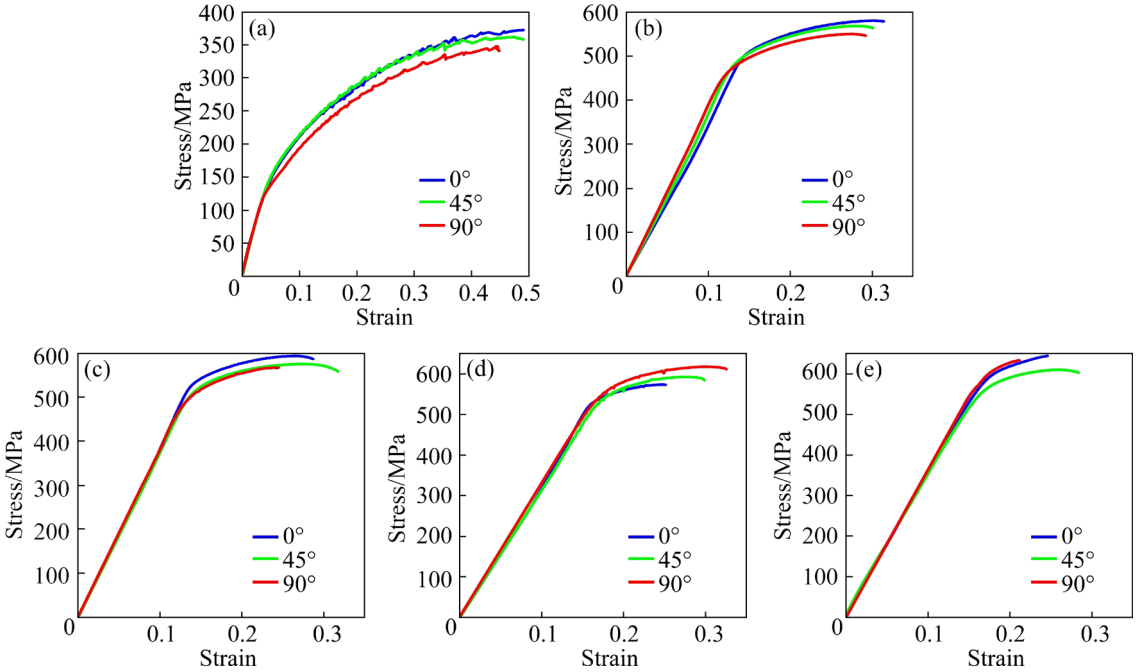

Fig. 12 Engineering stress−strain curves of 0% (solution-treated) (a), 10% (b), 20% (c), 40% (d), and 60% (e) rolled samples in RD (0°), HD (45°), and TD (90°)

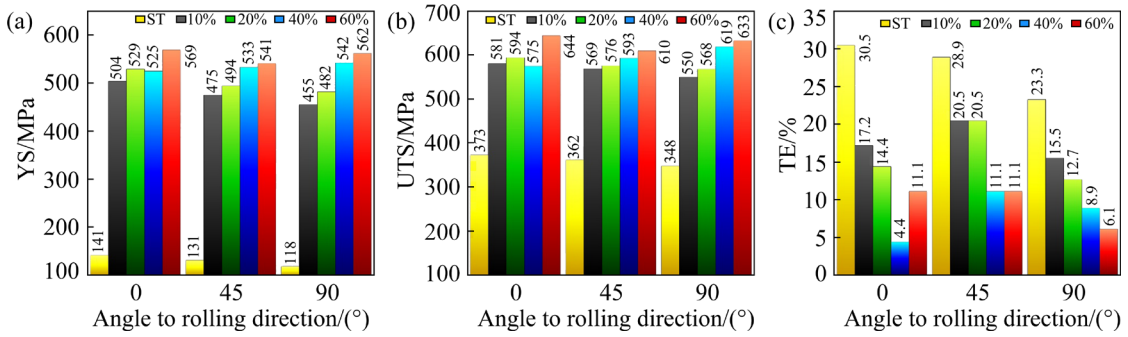

Fig. 13 Variations of YS (a), UTS (b), and TE (c) of solution-treated and rolled samples in RD, HD, and TD

strengthening components, i.e. Goss and Brass texture components, reach their highest values in this sample (see Fig. 10(d)). After 60% thickness reduction, the value of YS in the RD is higher than that in the TD. This also can be attributed to: (1) three orientations of [111], [110], and [103] with intensities of 1.1 versus one orientation of [110] with the intensity of 1.7 (Fig. 7 and Table 3); (2) the high value of the Copper component and low value of the Rotated Copper orientation in this sample (Fig. 10(e)). It should be noted that the values of YS in the HD are between the values of YS in RD and TD (Fig. 13(a)).

A parameter called in-plane anisotropy (IPA) is used to investigate and quantify anisotropy of tensile properties. To calculate the IPA, the following equation is utilized [6,7]:

$$\mathrm{IPA}=\frac{2\sigma_{\mathrm{y}}^{\max}-\sigma_{\mathrm{y}}^{\mathrm{mid}}-\sigma_{\mathrm{y}}^{\min}}{2\sigma_{\mathrm{y}}^{\max}}\times 100\% \tag{2}$$

where $\sigma_{\mathrm{y}}^{\max}$, $\sigma_{\mathrm{y}}^{\mathrm{mid}}$, and $\sigma_{\mathrm{y}}^{\min}$ are the highest, the middle, and the lowest values of YS, respectively.

The value of IPA is calculated based on the highest, the middle, and the lowest values of YS in three different directions of RD, HD, and TD. By using the data in Fig. 13(a), the IPA values for solution-treated and rolled samples have been calculated. The results are presented in Fig. 14. According to Table 5 and explanations previously discussed, Cube and Rotated Cube components reduce the magnitude of anisotropy, and Goss, Brass, Copper, S, and Rotated Copper components increase the amount of anisotropy. As shown in Fig. 14, the value of anisotropy for the 0% sample

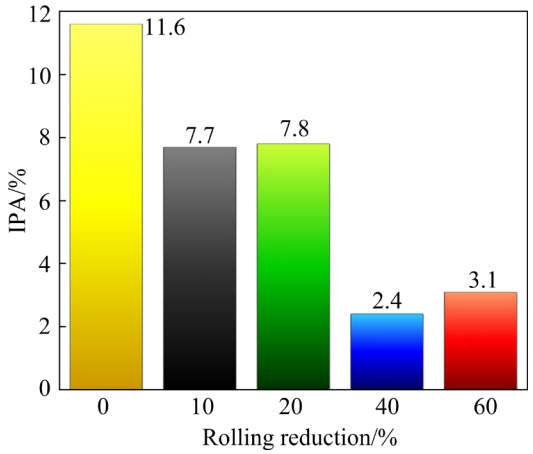

Fig. 14 IPA value as function of rolling reduction

is very high (high IPA value, equal to 11.6%). This result is due to: (1) the high intensity of Rotated Copper and Goss components; (2) the high maximum texture intensity of the solution- treated sample, which is equal to 11.5 (see Fig. 10(a)); (3) the existence of four orientations parallel to RD versus one orientation parallel to TD (Fig. 3). As shown in Fig. 14, the IPA values in 10% and 20% rolled samples decrease to 7.7% and 7.8%, respectively. This increment of isotropy may be due to the reduction of the maximum texture intensity to 6.8 and 8.8 in these samples (see Figs. 10(b) and (c)). The IPA in the 40% rolled sample reaches the lowest value, which is equal to 2.4%. This can be ascribed to the sharp increase in the intensity of the Rotated Cube component. The IPA value in the 60% rolled sample is still low (3.1%). This can be attributed to the low value of the maximum texture intensity, equal to 4.8 (see Fig. 10(e)). As a general rule in the present work, the IPA decreasing trend is in accordance with the maximum texture intensity trend (comparing Fig. 10 with Fig. 14). It should be noted that the formation of new equiaxed grains (see Fig. 11) in the 40% and 60% samples can reduce the value of anisotropy. It can be concluded that the SRDR process remarkably decreases the anisotropy of the AA7075 alloy.

To understand the effect of anisotropy on the work hardening of AA7075 alloy, the rate of strain hardening ($d\sigma/d\varepsilon$) for solution-treated and rolled samples in three different directions was calculated by the following equation [29−34]:

$$\frac{d\sigma}{d\varepsilon}=\frac{\sigma_{i+1}-\sigma_{i-1}}{\varepsilon_{i+1}-\varepsilon_{i-1}} \tag{3}$$

The strain hardening rate versus true strain curves of solution-treated and rolled samples in the directions of RD, HD, and TD are demonstrated in Fig. 15. As seen in Fig. 15(a), the strain hardening rate curves of the solution-treated sample in all directions have very large fluctuations, indicating

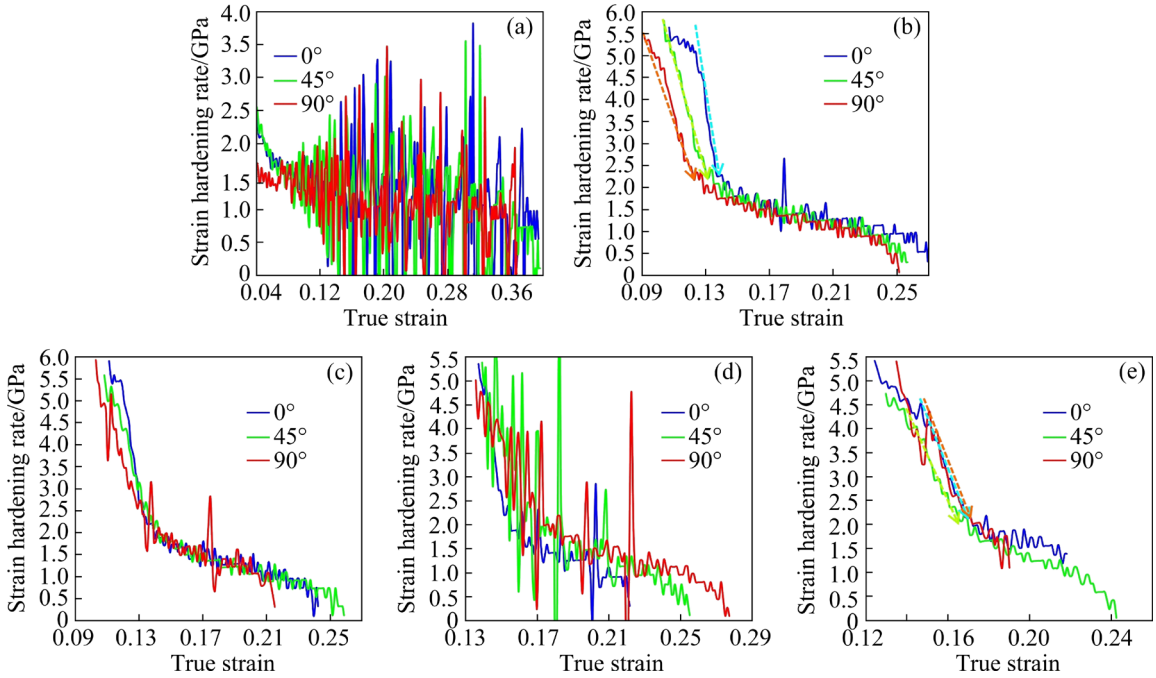

Fig. 15 Strain hardening rate−true strain curves of 0% (solution-treated) (a), 10% (b), 20% (c), 40% (d), and 60% (e) rolled samples in RD (0°), HD (45°), and TD (90°)

the occurrence of PLC. Figure 15(b) shows that the PLC effect is eliminated by only a 10% rolling reduction. From Fig. 15, with increasing the thickness reduction, the difference between strain hardening rate curves of RD, HD, and TD decreases as indicated by dashed orange arrows in Figs. 15(b) and (e). This is due to the decrement of texture intensity, consequently reduction in tensile anisotropy.

A very interesting point is the large fluctuation of strain hardening rate curves of the 40% rolled samples due to the PLC effect. As mentioned before, the new grains are formed after the 40% thickness reduction through the DRX phenomenon. With the occurrence of recrystallization, the density of dislocations decreases and this leads to the reappearance of the PLC instability. Another interesting point in the 40% sample is that the severity of PLC along the RD is much lower than that along the other two directions. With regard to Figs. 6(b), (d), and (f), this result can be ascribed to the presence of several strong orientations along the RD, whereas only one strong orientation can be observed along with the TD. This results in the activation of many slip systems at the beginning of the plastic deformation along RD, suppressing the easy movement of dislocations through interaction with the other dislocations. However, after the true strain of 0.17, the instability of curves along the RD increases due to easier cross-slip, recovery, and dislocation annihilation. Again, the presence of multiple orientations along the RD is responsible for the easier cross-slip at the end of the deformation.

The SEM images showing the fracture morphology of 0%, 10%, 20%, 40%, and 60% samples in RD, HD, and TD are depicted in Figs. 16−20, respectively. In general, the nucleation and propagation of microvoids, particle fracture, and interface decohesion (interfacial debonding) are the main fracture mechanisms of unprocessed and processed samples. As can be seen in Fig. 16, there are lots of large and small dimples, and tearing ridges throughout the fracture surface of the solution-treated sample. The fracture mode in this sample is totally ductile. By performing the SRDR process, the number and depth of dimples decrease and a transition from ductile to quasi-cleavage fracture has occurred. Regarding Fig. 13(c), the total elongation of the solution-treated sample in the RD (30.5%) is larger than that in the TD (23.3%). In agreement with the tensile result, the number and depth of dimples along the RD are higher than those along the TD, as shown in Figs. 16(a) and (e). It should be noted that the total elongations in 10% and 20% rolled samples in the TD are lower than those in the RD due to less ductile fracture in the TD (see Figs. 17 and 18). From Fig. 19, the fracture surface of samples along the RD is less ductile than that along the HD and TD, which is consistent with the ductility results in Fig. 13(c). In fact, the lowest

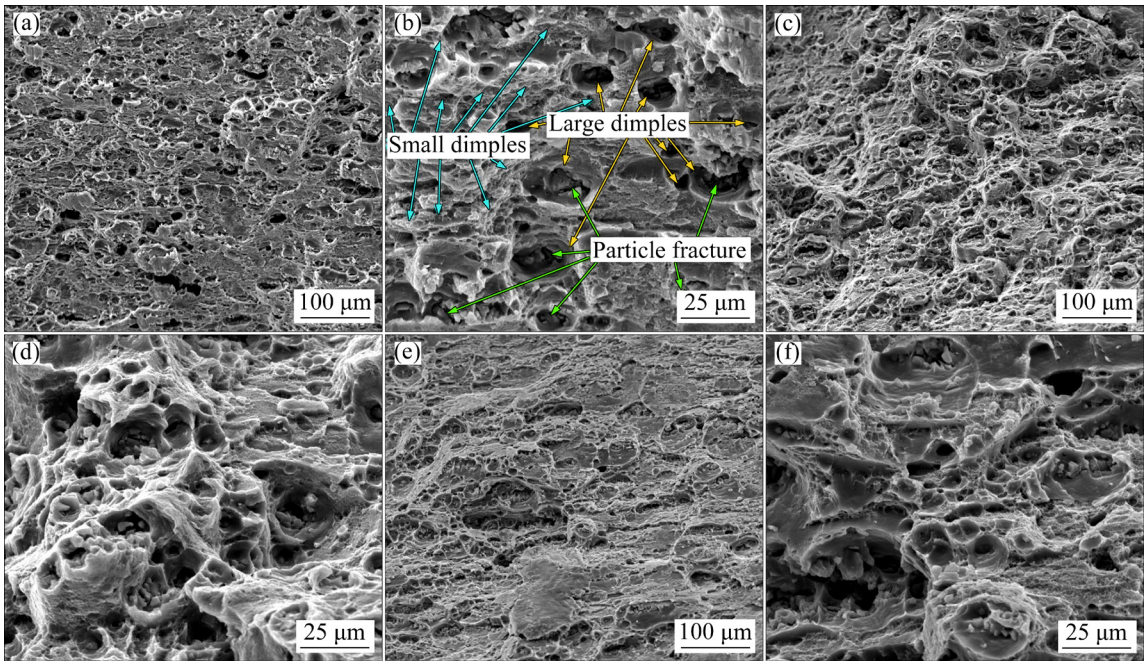

Fig. 16 SEM images showing fracture morphology of 0% (solution-treated) sample in RD (a, b), HD (c, d), and TD (e, f)

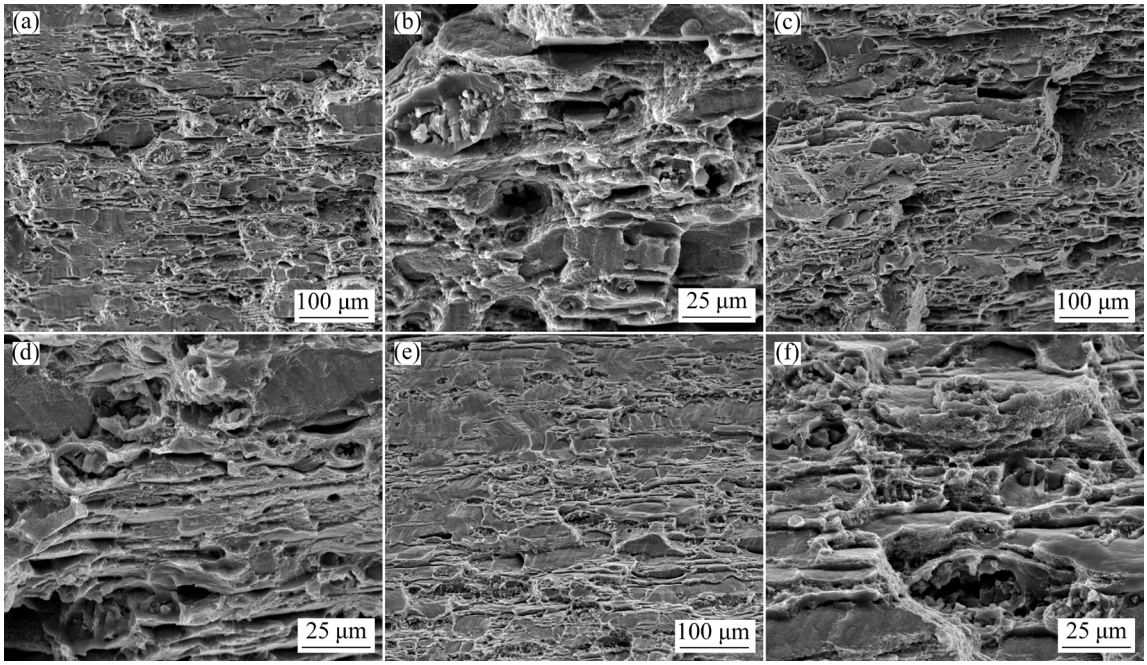

Fig. 17 SEM images showing fracture morphology of 10% rolled sample in RD (a, b), HD (c, d), and TD (e, f)

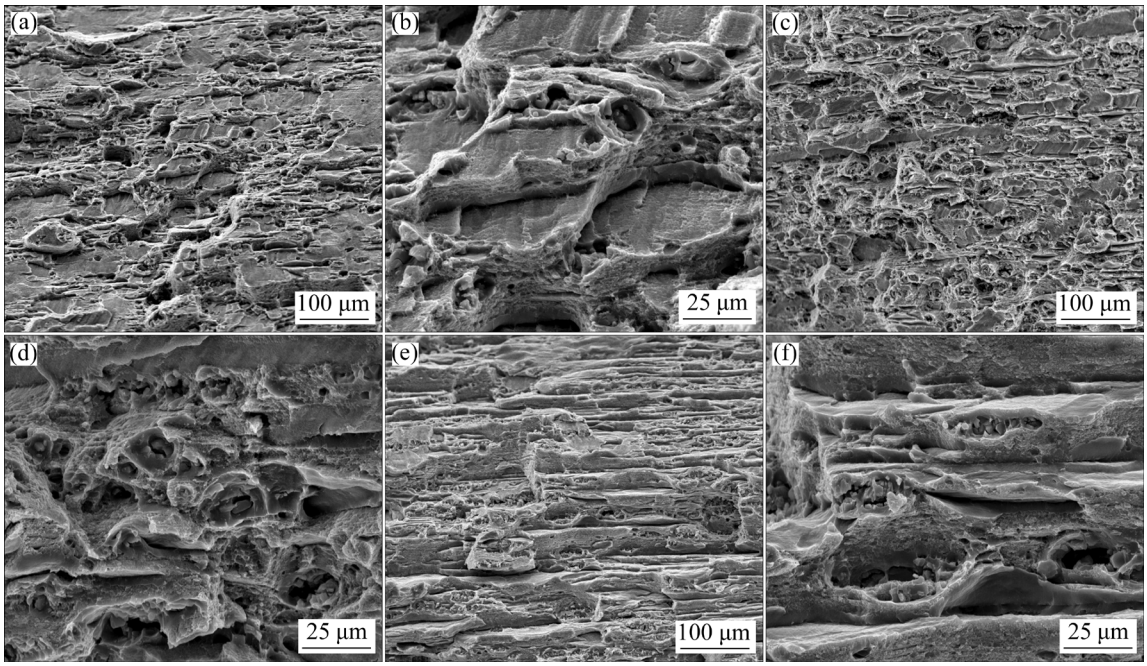

Fig. 18 SEM images showing fracture morphology of 20% rolled sample in RD (a, b), HD (c, d), and TD (e, f)

TE value (4.4%) belongs to the 40% rolled sample along the RD. This can be attributed to the severe strain hardening at the onset of plastic deformation caused by the presence of several orientations along the RD (see Figs. 6(b), (d), and (f)). As seen in Fig. 19(a), the fraction of particles on the fracture surface of the RD is much lower than that on the fracture surface of the HD and TD, indicating cleavage fracture mode owing to the intense strain hardening. From Fig. 20, there is no difference between the fracture surfaces of 60% samples in the RD, HD, and TD, revealing nearly isotropic fracture behavior in the AA7075 alloy. Based on the fractography results, it can be concluded that the anisotropy in the fracture surfaces decreases by performing the SRDR.

4 Conclusions

(1) The IPA value of Al−Zn−Mg−Cu alloy during single roll drive rolling was significantly reduced from 11.6% in solution-treated alloy to

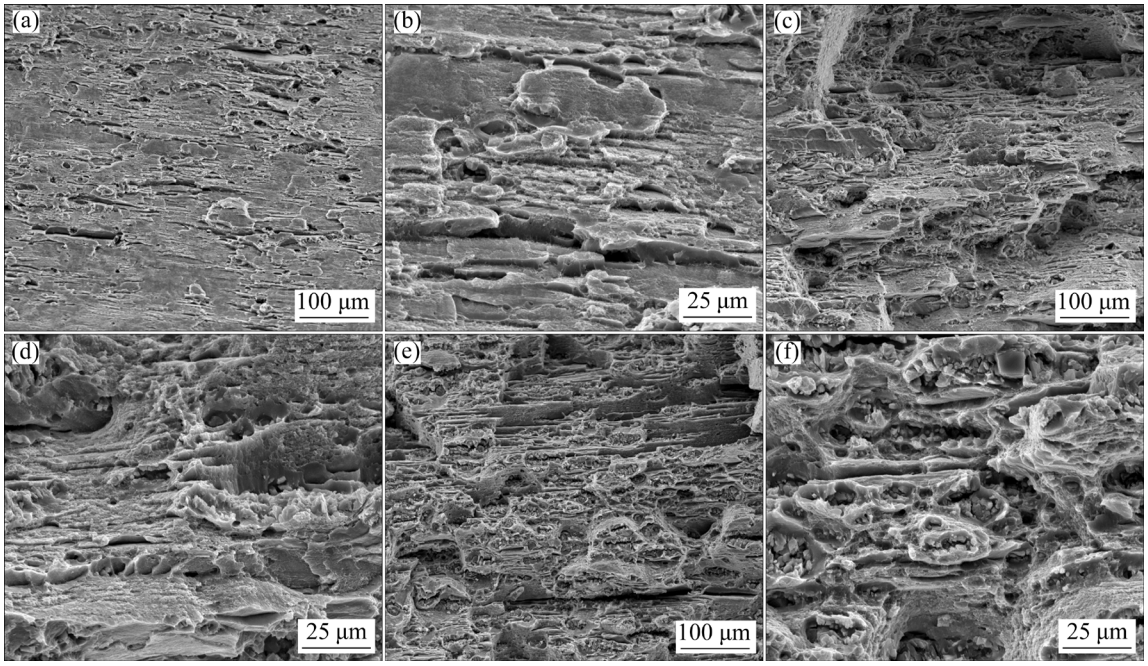

Fig. 19 SEM images showing fracture morphology of 40% rolled sample in RD (a, b), HD (c, d), and TD (e, f)

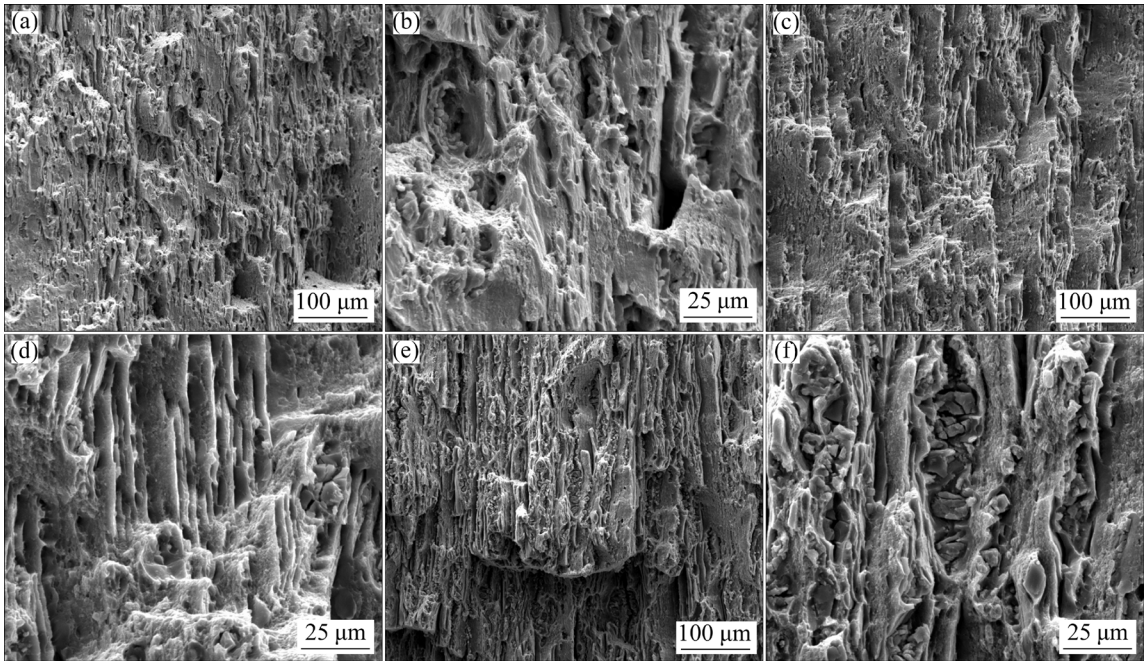

Fig. 20 SEM images showing fracture morphology of 60% rolled sample in RD (a, b), HD (c, d), and TD (e, f)

2.4% and 3.1% in 40% and 60% rolled samples, respectively. This was due to the formation of high-intensity Rotated Cube component, decrease of the maximum texture intensity, and formation of new grains through dynamic recrystallization.

(2) As a general rule in the present work, the IPA decreasing trend was in accordance with the maximum texture intensity trend.

(3) Except for the 40% rolled sample, in other samples, the yield strength in the RD was higher than the that in the TD, due to grain morphology and texture in these samples.

(4) The severity of PLC along the RD was much lower than that along the other two directions owing to the presence of several strong orientations along the RD.

(5) There was no difference between the fracture surfaces of 60% samples in the RD, HD, and TD, revealing nearly isotropic fracture behavior in the AA7075 alloy.

References

[1] HARPER C A. Handbook of materials for product design [M]. New York: McGraw-Hill, 2001.

[2] DAVIS J R. Alloying: Understanding the basics [M]. Ohio: ASM International, 2001.

[3] LEE Y S, KIM W K, JO D A, LIM C Y, KIM H W. Recrystallization behavior of cold rolled Al−Zn−Mg−Cu fabricated by twin roll casting [J]. Transactions of Nonferrous Metals Society of China, 2014, 24: 2226−2231.

[4] YUAN L L, GUO M X, YAN Y, FENG W J, LIU Z Y, ZHUANG L Z. Theoretical design and distribution control of precipitates and solute elements in Al−Zn−Mg−Cu alloys with heterostructure [J]. Transactions of Nonferrous Metals Society of China, 2021, 31: 3328−3341.

[5] ROUT M, PAL S K, SINGH S B. Cross rolling: A metal forming process [C]//Modern Manufacturing Engineering. Cham: Springer, 2015: 41−64.

[6] NAYAN N, MISHRA S, PRAKASH A, MURTY S V S N, PRASAD M J N V, SAMAJDAR I. Effect of cross-rolling on microstructure and texture evolution and tensile behavior of aluminium−copper−lithium (AA2195) alloy [J]. Materials Science and Engineering A, 2019, 740: 252−261.

[7] MONDAL C, SINGH A K, MUKHOPADHYAY A K, CHATTOPADHYAY K. Effects of different modes of hot cross-rolling in 7010 aluminum alloy: Part II. Mechanical properties anisotropy [J]. Metallurgical and Materials Transactions A, 2013, 44: 2764−2777.

[8] HUO W, HOU L, CUI H, ZHUANG L, ZHANG J. Fine-grained AA 7075 processed by different thermo-mechanical processings [J]. Materials Science and Engineering A, 2014, 618: 244−253.

[9] TAJALLY M, EMADODDIN E. Mechanical and anisotropic behaviors of 7075 aluminum alloy sheets [J]. Materials & Design, 2011, 32: 1594−1599.

[10] LI Z G, CHEN L, TANG J W, SUN W C, ZHAO G Q, ZHANG C S. Improving mechanical anisotropy and corrosion resistance of extruded AA7075 alloy by warm cross rolling and annealing [J]. Journal of Alloys and Compounds, 2021, 863: 158725.

[11] TOLOUIE E, JAMAATI R. Effect of β-$Mg_{17}Al_{12}$ phase on microstructure, texture and mechanical properties of AZ91 alloy processed by asymmetric hot rolling [J]. Materials Science and Engineering A, 2018, 738: 81−89.

[12] GOLI F, JAMAATI R. Effect of strain path during cold rolling on the microstructure, texture, and mechanical properties of AA2024 aluminum alloy [J]. Materials Research Express, 2019, 6: 066514.

[13] AMININEJAD A, JAMAATI R, HOSSEINIPOUR S J. Improvement of strength-ductility balance of SAE 304 stainless steel by asymmetric cross rolling [J]. Materials Chemistry and Physics, 2020, 256: 123668.

[14] SIDOR J, PETROV R H, KESTENS L A I. Deformation, recrystallization and plastic anisotropy of asymmetrically rolled aluminum sheets [J]. Materials Science and Engineering A, 2010, 528: 413−424.

[15] KAZEMI-NAVAEE A, JAMAATI R, JAMSHIDI AVAL H. Effect of single roll drive cross rolling on the microstructure, crystallographic texture, and mechanical behavior of Al–Zn–Mg−Cu alloy [J]. Archives of Civil and Mechanical Engineering, 2022, 22: 1−20.

[16] GOLI F, JAMAATI R. Asymmetric cross rolling (ACR): A novel technique for enhancement of Goss/Brass texture ratio in Al−Cu−Mg alloy [J]. Materials Characterization, 2018, 142: 352−364.

[17] AMININEJAD A, JAMAATI R, HOSSEINIPOUR S J. Achieving superior strength and high ductility in AISI 304 austenitic stainless steel via asymmetric cold rolling [J]. Materials Science and Engineering A, 2019, 767: 138433.

[18] WRONSKI S, BACROIX B. Microstructure evolution and grain refinement in asymmetrically rolled aluminium [J]. Acta Materialia, 2014, 76: 404−412.

[19] GOLI F, JAMAATI R. Intensifying Goss/Brass texture ratio in AA2024 by asymmetric cold rolling [J]. Materials Letters, 2018, 219: 229−232.

[20] TOLOUIE E, JAMAATI R. Effect of asymmetric cold rolling on the microstructure, texture, and mechanical properties of the AZ91 alloy [J]. Materials Research Express, 2018, 6: 036501.

[21] TAMIMI S, CORREIA J P, LOPES A B, AHZI S, BARLAT F, GRACIO J J. Asymmetric rolling of thin AA-5182 sheets: Modelling and experiments [J]. Materials Science and Engineering A, 2014, 603: 150−159.

[22] LIU W C, LI X Y, MENG X C. Effect of pseudo cross-rolling on the recrystallization texture of a continuous cast Al−Mg alloy [J]. Scripta Materialia, 2009, 60: 768−771.

[23] ZANCHETTA B D, DA SILVA V K, SORDI V L, RUBERT J B, KLIAUGA A M. Effect of asymmetric rolling under high friction coefficient on recrystallization texture and plastic anisotropy of AA1050 alloy [J]. Transactions of Nonferrous Metals Society of China, 2019, 29: 2262−2272.

[24] ZHANG J X, MA M, LIU W C. Effect of initial grain size on the recrystallization and recrystallization texture of cold-rolled AA5182 aluminum alloy [J]. Materials Science and Engineering A, 2017, 690: 233−243.

[25] SHUAI L F, HUANG T L, WU G L, HUANG X, MISHIN O V. Development of Goss texture in Al−0.3%Cu annealed after heavy rolling [J]. Journal of Alloys and Compounds, 2018, 749: 399−405.

[26] SHUAI L F, HUANG T L, WU G L, WINTHER G, HUANG X, MISHIN O V. Unusual through-thickness variations of microstructure and texture in heavily rolled and annealed Al−0.3%Cu [J]. Materials Characterization, 2020, 162: 110173.

[27] HERTZBERG R W, VINCI R P, HERTZBERG J L. Deformation and fracture mechanics of engineering materials [M]. 5th ed. Hoboken, NJ: John Wiley & Sons, 2012.

[28] LI Z, CHEN L, TANG J, ZHAO G, ZHANG C. Response of mechanical properties and corrosion behavior of Al−Zn−Mg alloy treated by aging and annealing: A comparative study [J]. Journal of Alloys and Compounds, 2020, 848: 156561.

[29] HASSANPOUR H, JAMAATI R, HOSSEINIPOUR S J. Effect of gradient microstructure on the mechanical properties of aluminum alloy [J]. Materials Characterization, 2021, 174: 111023.

[30] YAGHOOBI F, JAMAATI R, JAMSHIDI AVAL H. Simultaneous enhancement of strength and ductility in ferrite−martensite steel via increasing the martensite fraction [J]. Materials Chemistry and Physics, 2021, 259: 124204.
[31] ROODGARI M R, JAMAATI R, JAMSHIDI AVAL H. A new method to produce dual-phase steel [J]. Materials Science and Engineering A, 2021, 803: 140695.
[32] AFIFEH M, HOSSEINIPOUR S J, JAMAATI R. Effect of post-annealing on the microstructure and mechanical properties of nanostructured copper [J]. Materials Science and Engineering A, 2021, 802: 140666.
[33] YAGHOOBI F, JAMAATI R, JAMSHIDI AVAL H. A new 1.2 GPa-strength plain low carbon steel with high ductility obtained by SRDR of martensite and intercritical annealing [J]. Materials Science and Engineering A, 2020, 788: 139584.
[34] HASSANPOUR H, JAMAATI R, HOSSEINIPOUR S J. A novel technique to form gradient microstructure in AA5052 alloy [J]. Materials Science and Engineering A, 2020, 777: 139075.

单辊驱动轧制对 Al−5.6Zn−2.5Mg−1.4Cu 铝合金显微组织、织构和力学性能各向异性的影响

Amir KAZEMI-NAVAEE, Roohollah JAMAATI, Hamed JAMSHIDI AVAL

Department of Materials Engineering, Babol Noshirvani University of Technology, Shariati Ave., Babol 47148–71167, Iran

摘　要：研究在单辊驱动轧制 Al−5.6Zn−2.5Mg−1.4Cu 合金过程中，材料显微组织和织构的变化，并详细研究其力学性能各向异性与显微组织和织构的关系。对样品固溶处理后立即进行单辊驱动轧制，厚度减薄率分别为 10%、20%、40%和 60%。通过光学和扫描电子显微镜对显微组织进行表征，通过 X 射线衍射仪对织构进行表征，并对拉伸力学性能进行分析。结果表明，减薄率为 40%和 60%的轧制样品，其面内各向异性值从固溶处理合金的 11.6%分别显著降低到 2.4%和 3.1%。这是由于旋转立方织构的形成减小了总的织构强度以及动态再结晶过程中新晶粒的形成。由于样品中晶粒形貌和织构不同，样品轧制方向(RD)比横向(TD)的屈服强度高。沿 RD 存在的几个较强取向导致沿 RD (0°)的 Portevin–Le Chatelier (PLC)效应明显低于沿 HD (45°)和 TD (90°) 的。随着厚度减薄率的增大，织构强度减小，导致 RD、HD 和 TD 之间的应变硬化率差异减小。而对于减薄率为 60%的样品，其 RD、HD 和 TD 的断裂面无差异，说明其断裂行为为各向同性。

关键词：AA7075 铝合金；单辊驱动轧制；织构；力学性能；各向异性

(Edited by Wei-ping CHEN)